ACS APPLIED MATERIALS & INTERFACES

Research Article

www.acsami.org

# Efficient Visible-Light Photocatalytic Hydrogen Evolution and Enhanced Photostability of Core/Shell CdS/g-$C_3N_4$ Nanowires

Jiye Zhang,[†] Yonghao Wang,[†] Jian Jin,[‡] Jun Zhang,[‡] Zhang Lin,[§] Feng Huang,*[,†] and Jiaguo Yu*[,‡]

[†]Key Laboratory of Optoelectronic Materials Chemistry and Physics, Fujian Institute of Research on the Structure of Matter, Chinese Academy of Sciences, Fuzhou, Fujian 350002, China

[‡]State Key Laboratory of Advanced Technology for Material Synthesis and Processing, Wuhan University of Technology, Luoshi Road 122#, Wuhan, Hubei 430070, China

[§]State Key Lab of Structural Chemistry, Fujian Institute of Research on the Structure of Matter, Chinese Academy of Sciences, Fuzhou, Fujian 350002, China

Supporting Information

**ABSTRACT:** CdS/g-$C_3N_4$ core/shell nanowires with different g-$C_3N_4$ contents were fabricated by a combined solvothermal and chemisorption method and characterized by X-ray powder diffraction, scanning electronic microscopy, transmission electron microscopy, and UV−vis diffuse reflection spectroscopy. The photocatalytic hydrogen-production activities of these samples were evaluated using $Na_2S$ and $Na_2SO_3$ as sacrificial reagents in water under visible-light illumination ($\lambda \geq 420$ nm). The results show that after a spontaneous adsorption process g-$C_3N_4$ is successfully coated on CdS nanowires with intimate contact and can significantly improve the photocatalytic hydrogen-production rate of CdS nanowires, which reaches an optimal value of up to 4152 $\mu$mol $h^{-1}$ $g^{-1}$ at the g-$C_3N_4$ content of 2 wt %. More importantly, g-$C_3N_4$ coating can substantially reinforce the photostability of CdS nanowires even in a nonsacrificial system. The synergic effect between g-$C_3N_4$ and CdS, which can effectively accelerate the charge separation and transfer corrosive holes from CdS to robust $C_3N_4$, was proposed to be responsible for the enhancement of the photocatalytic activity and photostability. The possible conditions necessary for the synergic effect to work in a CdS/g-$C_3N_4$ core/shell configuration is also discussed.

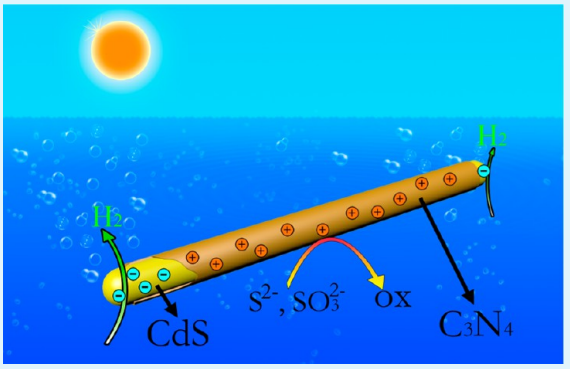


**KEYWORDS:** *solar fuels, photocatalysis, hydrogen production, CdS nanowire, carbon nitride, charge transfer*

## INTRODUCTION

With the depletion of fossil-fuel reserves, an urgent challenge confronting human beings is to seek a clean and sustainable alternative-energy source.[1] Solar fuels,[2,3] including hydrogen from water splitting[4−6] and carbon-based fuels from aqueous $CO_2$ reduction,[7−10] which store the energy from the incident solar irradiation in their chemical bonds, may provide the most viable solution. Compared with solar-photovoltaic energy, solar fuels have the advantages of being unintermittent in supply, easy to be stored, and in some cases compatible with the present industrial system.[6,11] Inspired by natural photosynthesis, various semiconductors, such as $TiO_2$,[12−16] ZnS,[17−20] and others, were extensively investigated as light absorbers and photocatalysts in the artificial light-driving water splitting and $CO_2$ reduction. Among them, CdS is considered to be a fascinating visible-light photocatalyst for hydrogen evolution because of its desired band-gap width (2.4 eV) and suitable band-edge positions.[21,22] However, before CdS can become practically useful in large-scale hydrogen production, there are two major obstacles should be tackled. First, the photocatalytic efficiency of CdS is severely restricted by the fast recombination of photoexcited charge carriers.[23] Even worse, as frequently reported, CdS seriously suffers from photocorrosion under strong illumination. $S^{2-}$ in CdS tends to be self-oxidized by photogenerated holes before the oxidation of water.[1,21,24]

Hence, enormous efforts have been dedicated to either reducing the recombination of photogenerated charge carriers or inhibiting the photocorrosion of CdS. For instance, CdS was coupled with various semiconductors ($TiO_2$, ZnO, $Ta_2O_5$, etc.)[25−27] or noble metals[28,29] to introduce a strong interface electric field by band-edge offset, which can effectively accelerate the separation of photogenerated charge carriers. However, to address the issue of photocorrosion, several approaches were proposed. One is that CdS can be protected by being coated with or encapsulated into amorphous carbon[30] or polymeric materials, such as conducting polyaniline (PANI)[31] and polystyrene-divinylbenzene resin.[32] Another is that robust $O_2$ production materials, such as $RuO_2$ and $IrO_2$,[33]

Received: August 10, 2013
Accepted: September 20, 2013
Published: September 20, 2013

  

can be loaded on CdS as hole trappers and thus alleviate the damage to CdS by photogenerated holes. Recently, a polymeric photocatalyst, the so-called graphitic carbon nitride (g-$C_3N_4$), has attracted much attention because of its abundance, high thermal and chemical stability, and visible-light response.[34−37] Graphene-like ultrathin g-$C_3N_4$ nanosheets were reported to exhibit improved performance for photocatalysis or biosensing because of the large surface area and fast charge transfer.[38−40] However, it was proposed that as a $\pi$-conjugated material, hybridizing g-$C_3N_4$ with various nanomaterials can effectively improve their photocatalytic activities and visible-light responses.[41−43] More importantly, g-$C_3N_4$ is the most stable allotrope of carbon nitrides, which exhibit good durability in varied chemical environments.[35] In addition, when examining the band-edge position of CdS and g-$C_3N_4$, it was found that corrosive photogenerated holes in CdS can readily transfer to $C_3N_4$ because of the lower valence band maximum of CdS versus the HOMO level of $C_3N_4$.[44−46] Therefore, it can be speculated that combining CdS with g-$C_3N_4$ may provide a feasible solution to deal with its drawbacks of low efficiency and poor photostability simultaneously.

In this article, we present a g-$C_3N_4$/CdS hybrid system fabricated by a solvothermal and chemisorption method. CdS nanowires were chosen as the host material for $C_3N_4$ loading, which themselves may exhibit superior photocatalytic activities owing to the high crystallinity and the fast electron transport in a 1D structure.[29,47] Considering its graphitic-like structure, g-$C_3N_4$ can easily be exfoliated into thin sheets by a simple ultrasonic method[42] and then self-assembly-coated on CdS nanowires to form a core/shell configuration with intimate contact. The physicochemical properties as well as the photocatalytic $H_2$-production rate from aqueous solutions containing $Na_2S$ and $Na_2SO_3$ of these CdS/g-$C_3N_4$ core/shell nanowires were extensively characterized and investigated. The photocorrosion behaviors of the pristine and g-$C_3N_4$-coated CdS nanowires in a nonsacrificial system were also investigated. It can be found that after g-$C_3N_4$ coating, the photocatalytic efficiency and photostability of the CdS nanowires were substantially improved. The role of $C_3N_4$ in the photocatalytic hydrogen-production process and its optimum content were discussed and illustrated. This work may provide a stepping stone towards the practical application of CdS in photocatalytic hydrogen production.

## EXPERIMENTAL SECTION

**Chemicals.** All of the chemicals (AR grade) in this work, including $Cd(NO_3)_2{\cdot}4H_2O$, thiourea, ethylenediamine, dicyandiamide, barbituric acid (BA), $Na_2S{\cdot}9H_2O$, and $Na_2SO_3$, were purchased from Aladdin Reagent Co. Ltd. and were used without any further purification.

**Fabrication of CdS/g-$C_3N_4$ Core/Shell Nanowires.** First, CdS nanowires were synthesized by a solvothermal method.[48] Briefly, 0.641 g of $Cd(NO_3)_2{\cdot}4H_2O$ and 0.474 g of thiourea were added into a dried Teflon-lined autoclave with a capacity of 20 mL. After 10 mL of ethylenediamine was injected, the autoclave was sealed and heated at 180 °C for 72 h and then rapidly quenched to room temperature after the solvothermal reaction. The obtained yellow precipitates were centrifuged, rinsed with ethanol and distilled water five times, and then dried in a vacuum oven at 60 °C. Modified g-$C_3N_4$ was prepared by copolymerization.[36] Three grams of dicyandiamide and 0.15 g of BA were mixed in 15 mL of water and heated at 90 °C with stirring until all water was evaporated, leaving a white solid. The white solids were calcined at 550 °C for 4 h in air to obtain bulk g-$C_3N_4$. Copolymerization with an appropriate amount of BA can introduce substitutional carbon atoms into the nitrogen sites of g-$C_3N_4$, which extended the optical absorption range of $C_3N_4$ and thus improved its photocatalytic performance.

CdS/g-$C_3N_4$ core/shell nanowires were fabricated via a two-step self-assembly procedure.[42] A measured amount of as-prepared bulk g-$C_3N_4$ was grounded to fine powder and then added into 25 mL of methanol. After being ultrasonically treated for 30 min, bulk g-$C_3N_4$ was exfoliated into thin sheets and disintegrated into a homogeneous suspension. CdS nanowires were then dispersed in the suspension and stirred at room temperature for 24 h. The residual methanol was removed by a stream of nitrogen. The obtained yellow solid was collected and dried in a vacuum oven at 60 °C. The nominal weight ratios of $C_3N_4$ to CdS ($R_{CN}$) were 0, 0.5, 1, 2, 3, and 4 wt %, and the samples were labeled as CN0 (pristine CdS nanowire), CN0.5, CN1, CN2, CN3, and CN4, respectively.

**Characterization.** X-ray powder diffraction was used to identify the crystal structures and phase compositions of the samples. Diffraction data were collected on a PANalytical X'Pert PRO diffractometer with an X'Celerator detector using Cu K$\alpha$ radiation (40 kV × 40 mA). The 2$\theta$ scanning range was from 5° to 85° with a scanning speed of 4°/min in the continuous mode. Scanning electronic microscopy (SEM, JEOL, JSM-6700F equipped with an Oxford energy-dispersive X-ray spectrometer (EDS)) was used to determine the size and morphology of the samples. Further morphological and structural characterizations were based on transmission electron microscopy (TEM), high-resolution transmission microscopy (HRTEM) observation, and selected area electron diffraction (SAED). TEM/HRTEM imaging and SAED were conducted on a FEI Tecnai G2 F20 field-emission transmitting electron microscope at an acceleration voltage of 200 kV. X-ray photoelectron spectroscopy (XPS) measurements were done on a Thermo Scientific ESCALAB 250 instrument with Al K$\alpha$ source. The nitrogen adsorption and desorption isotherms at 77 K were measured using a Micrometrics ASAP 2020 system after the samples were degassed in vacuum at 120 °C overnight. The Brunauer−Emmett−Teller (BET) surface area was determined by a multipoint BET method using adsorption data in the relative pressure ($P/P_0$) range of 0.05−0.25. Diffuse reflectance UV−vis spectra of the samples were collected using a Shimadzu UV-2550 UV−vis spectrophotometer equipped with an integrating sphere. $BaSO_4$ was the reference sample. The absorption spectra can be further calculated from the reflectance spectra using the Kubelka−Munk function, $K/S = (1 - R)^2/2R$, where $K$ is the absorption coefficient, $R$ is the diffused reflectance, and $S$ is the scattering coefficient.

**Photocatalytic $H_2$-Production Activity and Photocorrosion Behavior.** The photocatalytic hydrogen-production experiments were performed in a 100 mL three-necked Pyrex flask at ambient temperature and atmospheric pressure, and the outlets of the flask were sealed with a silicone rubber septum. A 350 W xenon arc lamp with a UV cutoff filter ($\lambda \geq 420$ nm), which was positioned 20 cm away from the reactor, served as the irradiation light source to trigger the photocatalytic reaction. The focused intensity on the flask was about 180 mW cm$^{-2}$. In a typical photocatalytic experiment, 50 mg of catalyst was dispersed in 80 mL of a mixed aqueous solution containing 0.35 M $Na_2S$ and 0.25 M $Na_2SO_3$, and the system was then bubbled with nitrogen for 40 min to remove the dissolved oxygen and create an anaerobic condition. Pt cocatalyst (0.6 wt %) was photodeposited on the catalysts by directly dissolving $H_2PtCl_6$ into the reactant suspension. During irradiation, continuous stirring was applied to keep the photocatalyst particles in suspension. Gas (0.4 mL) was intermittently sampled through the septum, and hydrogen was analyzed by a gas chromatograph (Shimadzu GC-14C, with nitrogen as a carrier gas) equipped with a 5 Å molecular-sieve column and a thermal-conductivity detector. All glassware was carefully rinsed with distilled water prior to use. The apparent quantum efficiency (QE) was measured under the same photocatalytic reaction condition. Four low-power 420 nm LEDs (3 W) (Shenzhen Lamplic Science Co. Ltd.) were used as the irradiation light sources. The LEDs were positioned 1 cm away from the reactor in four different directions, and the focused intensity for each LED was ca. 6 mW cm$^{-2}$. The QE was calculated according to eq 1:

$$\text{QE}\ (\%) = \frac{\text{number of reacted electrons}}{\text{number of incident photons}} \times 100$$
$$= \frac{\text{number of evolved } H_2 \text{ molecules} \times 2}{\text{number of incident photons}} \times 100 \quad (1)$$

The photocorrosion behaviors of the selected samples in a nonsacrificial system were investigated in a gas-closed reactor with water cooling. An assembling quartz window (60 mm in diameter) on the top of the reactor was used for light entrance. Fifty milligrams of the sample was dispersed in 100 mL of distilled water, and the system was bubbled with nitrogen for 40 min to create an anaerobic condition. The suspension was irradiated by a 350 W xenon arc lamp with continuous stirring. At certain time intervals, 2 mL aliquots were sampled and centrifuged at 13 000 rpm for 5 min to separate the solutions and catalysts. The concentration of released $Cd^{2+}$ in the reaction solution was determined by inductively coupled plasma atomic emission spectrometry (ICP-AES, Jobin Yvon Ultima2). The separated catalysts were also characterized by TEM observation. No Pt cocatalysts were used in the photocorrosion tests.

**Photoelectrochemical Measurements.** Photocurrent measurements were performed on a CHI 660D electrochemical workstation (Chenhua Instrument, Shanghai, China) in a conventional three-electrode configuration with a Pt foil as the counter electrode and a Ag/AgCl (saturated KCl) reference electrode. A 300 W Xe arc lamp severed as a light source. A 0.5 M $Na_2SO_4$ aqueous solution was used as the electrolyte. The working electrodes were prepared as follows: 10 mg of the prepared photocatalyst was ground with 20 $\mu$L of a PEDOT-PSS (Sigma-Aldrich, 1.3−1.7%) aqueous solution and 100 $\mu$L of distilled water to make a slurry. The slurry was then spread on a 2 × 0.5 $cm^2$ ITO glass substrate with an active area of about 0.5 $cm^2$ by the doctor-blade method, using adhesive tape as the space. The film was dried in air and annealed at 150 °C for 30 min in a flowing $N_2$ atmosphere. The photoresponses of the samples as light on and off were measured at 0.0 V.

## RESULTS AND DISCUSSION

**Phase Structure and Morphology.** The crystal structure and phase composition of the samples were characterized by XRD. Figure 1a shows the XRD patterns of CdS/$C_3N_4$ samples with different $C_3N_4$ contents together with those of the pure CdS (CN0) and $C_3N_4$. XRD data of CN0 indicate that the as-prepared pure CdS is crystallized in hexagonal wurtzite structure with the space group *P*63*mc* and lattice parameters $a$ = 4.132 Å and $c$ = 6.734 Å (JCPDS no. 65-3414). Interestingly, the relative intensity of the (002) peak of the CdS sample is remarkably low compared with the standard diffraction data, indicating that the material is growing preferentially along the direction of the $c$ axis, which lies mostly parallel to the experimental plane during XRD measurements. Pure $C_3N_4$ shows two distinct diffraction peaks at 13.2° and 27.4°, corresponding to the (100) and (002) peaks of the graphitic phase, respectively.[49] After $C_3N_4$ loading, no notable difference was found in the XRD patterns of the CdS materials because of the low content (< 4 %) and the low X-ray diffraction intensity of $C_3N_4$. Nevertheless, the presence of g-$C_3N_4$ could be confirmed by EDS and XPS analyses when its content was increased to 8 wt % (see the Supporting Information, Figures S2 and S3, and the discussions therein).

The detailed characterization of the morphologies and crystal structures of the samples was based on SEM, TEM/HRTEM, and SAED. Figure 1b presents the SEM image of the pristine CdS sample, and the inset is the corresponding TEM image. It can be seen that the morphology of pristine CdS is well-crystallized nanowires with lengths of 2−4 $\mu$m and diameters of

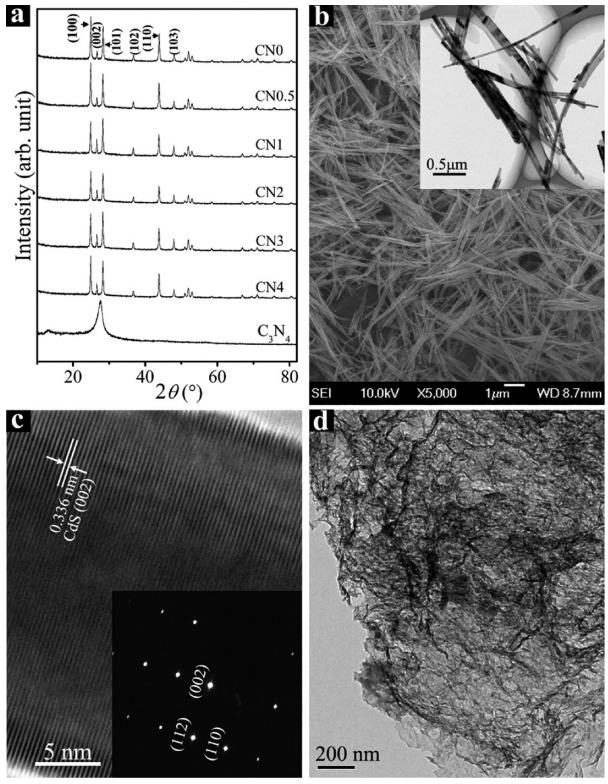


**Figure 1.** (a) XRD patterns of CNX (X = 0, 0.5, 1, 2, 3, and 4) together with that of the pure g-$C_3N_4$. (b) SEM image of CN0 (the inset is the corresponding TEM image). (c) HRTEM image of a typical CdS nanowire (the inset is the SAED pattern). (d) TEM image of g-$C_3N_4$ sheets after ultrasonic treatment.

about 50 nm. The HRTEM image in Figure 1c reveals that the distances between the adjacent lattice fringes in the growth direction are about 0.336 nm, in agreement with the (002) d spacing for bulk CdS. The SAED pattern (the inset in Figure 1c) can be indexed as the [2$\bar{2}$0] zone axis of a hexagonal wurtzite structure. It can be inferred that the CdS nanowires were single crystalline and predominantly growing along the $c$ axis, which is consistent with the results of XRD. Figure 1d displays the TEM image of the thin $C_3N_4$ sheet after ultrasonic exfoliation in methanol (see also Figure S1 in the Supporting Information).

The morphological and structural features of the CdS/g-$C_3N_4$ samples were further examined by TEM/HRTEM. From Figure 2a,b, it can be seen that after a spontaneous adsorption process $C_3N_4$ is successfully coated on CdS nanowires with intimate contact, and the core/shell structures can be clearly observed in the TEM image because of the different electron penetrability between the cores and shells. In the HRTEM image (Figure 2c), besides the lattice fringes with d spacing of 0.67 nm belonging to CdS,[48] a different kind of lattice fringes with d spacing of 0.326 nm can be found in the shell region, which corresponds to the typical (002) interlayer-stacking distance of g-$C_3N_4$.[42] Through TEM observation, it can be inferred that the exfoliated $C_3N_4$ sheets are preferentially coated on the lateral surface of the nanowires to achieve a minimum surface energy. Therefore, at low $R_{CN}$ (Figure 2a), g-$C_3N_4$ forms a thin and unclosed shell, leaving the tips and some areas of the CdS nanowire uncovered. With $R_{CN}$ increasing, the coated $C_3N_4$ gets thicker and gradually forms a completely closed shell (Figure 2b). The thickness of the $C_3N_4$ layer is

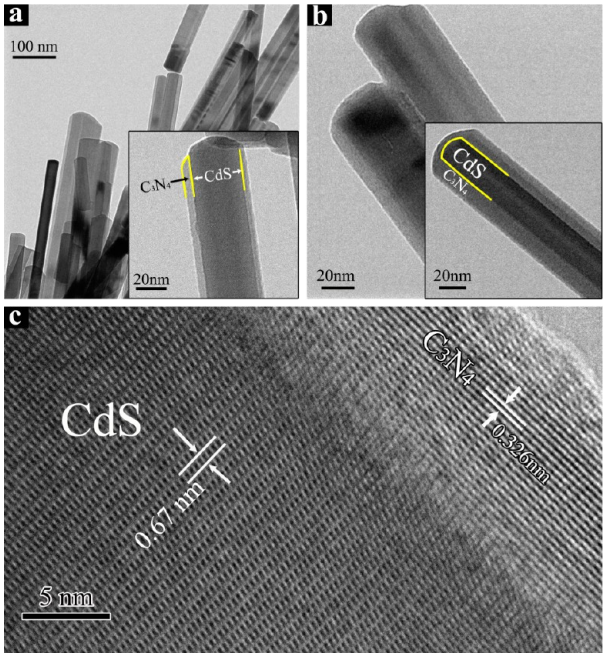


**Figure 2.** TEM images of (a) CN2 and (b) CN4, and (c) HRTEM image of CN4.

about 5 nm for CN2, whereas for CN4, it is about 15 nm. The formation of the $C_3N_4$ shell may involve an initial adsorption of fractional g-$C_3N_4$ sheets and the following reassembly process (see the Supporting Information, Figure S4). During the process, CdS nanorods can be considered as templates for the self-assembly of g-$C_3N_4$ nanosheets. First, g-$C_3N_4$ nanosheets adsorb on the surface of CdS nanorods to minimize the total interfacial energy. It was reported that in methanol, g-$C_3N_4$ nanosheets tend to undergo a rolling mechanism and a regrowth process.[50] Therefore, in our reaction system, g-$C_3N_4$ nanosheets could curl up and wrap around the CdS nanorods. Then, as the reaction in methanol solution continues, the adsorbed g-$C_3N_4$ nanosheets will reassemble into a smooth and homogeneous layer.

**UV–Vis Absorption Properties.** Figure 3 depicts the UV–vis diffuse absorption spectra for samples CN0, CN0.5, CN1, CN2, CN3, CN4, and g-$C_3N_4$. As shown in Figure 3, the as-prepared g-$C_3N_4$ shows a much broader absorption range compared with those in the literature.[46] In this work, g-$C_3N_4$

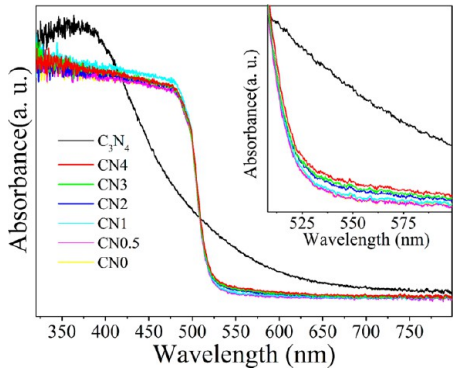


**Figure 3.** Comparison of UV–vis absorbance spectra of the prepared g-$C_3N_4$, pristine CdS nanowires (CN0), and g-$C_3N_4$ coated CdS nanowires (CN0.5, CN1, CN2, CN3, and CN4).

was synthesized by a reported copolymerization method.[36] During the copolymerization process, BA could introduce carbon atoms into the melon-based carbon nitride structures by replacing one of the ring nitrogen atoms, which changes the electronic structure of g-$C_3N_4$ and thus extends its optical absorption range. However, g-$C_3N_4$ coating does not significantly change the optical absorption feature of CdS nanowires. The band gaps of the samples were further determined by fitting the optical transition at the absorption edges using the Tauc/David–Mott model[51] described by the equation $(h\nu\alpha)^{1/n} = A(h\nu - E_g)$, where $h$ is the Planck's constant, $\nu$ is the frequency of vibration, $\alpha$ is the absorption coefficient, $E_g$ is the band gap, and $A$ is a proportional constant. The value of the exponent $n$ denotes the nature of the sample transition and is defined to be 0.5 for a directly allowed transition. The fitting results indicate that the band gap of the prepared modified g-$C_3N_4$ is about 2.6 eV, which is consistent with the existing results.[36] Meanwhile, the band gap of CdS remains unchanged after g-$C_3N_4$ coating and was determined to be about 2.4 eV for all of the CdS/g-$C_3N_4$ samples. Nevertheless, because of the relatively high optical absorption coefficient of g-$C_3N_4$ in the wavelength range of 520–800 nm, the absorbances of CdS/g-$C_3N_4$ are slightly enhanced with the increasing g-$C_3N_4$ contents in such a wavelength region (inset in Figure 3).

**BET Surface Areas and Pore Size Distributions.** Figure 4 shows the nitrogen adsorption–desorption isotherms at 77 K

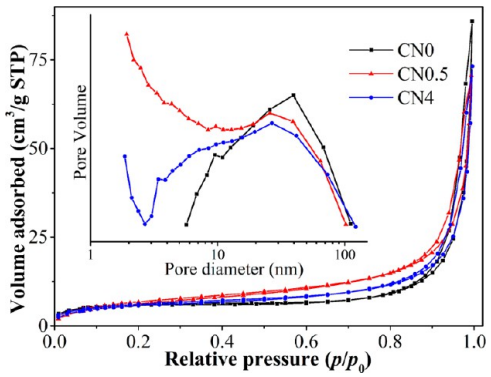


**Figure 4.** Nitrogen adsorption–desorption isotherms and the corresponding pore size distributions (the inset) calculated by the BJH method for CN0, CN0.5, and CN4.

and the obtained pore size distributions by BJH method (the inset) for CN0, CN0.5, and CN4. It can be seen that the nitrogen adsorption–desorption isotherms of these three samples are similar and all of them are type IV with hysteresis loops according to the IUPAC classification,[52] indicating the presence of mesopores. In addition, the adsorption branches of these isotherms increase rapidly at relative pressures close to unity, which bear some resemblance to type II isotherms. Therefore, the samples also possess large macropores. All of the hysteresis loops can be categorized as type H3, suggesting the existence of slit-like pores. The BET specific surface areas, pore volumes, and average pore sizes of all of the samples are summarized in Table 1. As listed in Table 1, the BET specific surface area ($S_{BET}$) of the pristine CdS nanowires is about 20.5 $m^2\ g^{-1}$. After 0.5 wt % g-$C_3N_4$ is coated, the $S_{BET}$ of CN0.5 increased to 25.5 $m^2\ g^{-1}$. However, when the $C_3N_4$ content is further increased, the $S_{BET}$ of the samples become smaller. The variations in $S_{BET}$ may relate to the changes in pore size

**Table 1. Effects of $R_{CN}$ on the Physical Properties and Photocatalytic Activities of the Samples**

| samples | $R_{CN}$ (%) | $S_{BET}$ ($m^2\ g^{-1}$) | pore volume ($cm^3\ g^{-1}$) | average pore size (nm) | activity ($\mu mol\ h^{-1}\ g^{-1}$) | QE (%) |
|---|---|---|---|---|---|---|
| CN0 | 0 | 20.5 | 0.13 | 38.7 | 2001 | 2.1 |
| CN0.5 | 0.5 | 25.5 | 0.11 | 20.5 | 1982 | 2.0 |
| CN1 | 1 | 23.6 | 0.10 | 22.2 | 2659 | 2.7 |
| CN2 | 2 | 22.9 | 0.11 | 25.7 | 4152 | 4.3 |
| CN3 | 3 | 22.7 | 0.11 | 27.6 | 1030 | 1.1 |
| CN4 | 4 | 21.8 | 0.11 | 29.8 | 470 | 0.5 |

distribution. As can be seen in the inset of Figure 4, the pristine CdS nanowires contain both mesopores (6−50 nm) and macropores (50−110 nm). The presence of small amount of g-$C_3N_4$ (0.5 wt %) can introduce a lot of small mesopores (2−10 nm) and thus decrease the average pore size from 38.7 (for CN0) to 20.5 nm (for CN0.5). By considering that the pore volumes of all of the samples do not change appreciably, the $S_{BET}$ of CN0.5 will increase accordingly. However, a further increase of the $C_3N_4$ content may lead to the adhesion and aggregation of the CdS nanowires, which in turn reduces the small mesopores (see the pore size distribution for CN4) and then increases the average pore size. Consequently, the $S_{BET}$ of the samples will decrease.

**Photocatalytic Activity and Photostability.** Photocatalytic $H_2$-production activities of the CdS/g-$C_3N_4$ core/shell nanowires were evaluated under visible-light ($\lambda \geq 420$ nm) irradiation using mixed 0.35 M $Na_2S$ and 0.25 M $Na_2SO_3$ aqueous solutions as scavenger. Pt (0.6 wt %) was added as a cocatalyst to reduce the overpotential for hydrogen evolution. The results are shown in Figure 5 and Table 1. As can be seen,

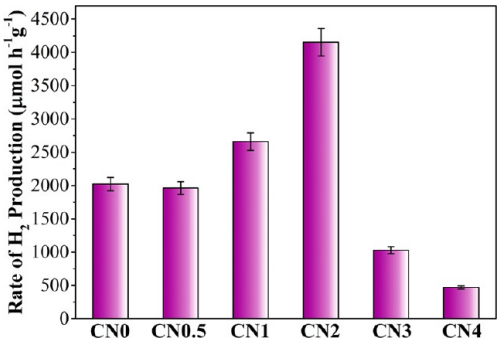


**Figure 5.** Comparison of photoatalytic $H_2$-production activities of pristine CdS nanowires (CN0) and g-$C_3N_4$-coated CdS nanowires (CN0.5, CN1, CN2, CN3, and CN4) from mixed 0.35 M $Na_2S$ and 0.25 M $Na_2SO_3$ aqueous solutions.

the pristine CdS nanowires exhibit a relatively high $H_2$-production activity up to 2001 $\mu mol\ h^{-1}\ g^{-1}$, which may be credited to their high crystallinity and the fast electron transport in 1D structures. Coating the CdS nanowires with a small amount of g-$C_3N_4$ can substantially improve the hydrogen-production activity. The optimal photocatalytic activity was achieved at 2 wt % g-$C_3N_4$ content, and the hydrogen-production rate reached 4152 $\mu mol\ h^{-1}\ g^{-1}$ with an apparent quantum efficiency (QE) of up to 4.3% at 420 nm (for CN2). However, further increasing of $R_{CN}$ to 4 wt % leads to a reduction of the photocatalytic activity, which is less than one-fourth of that for the pristine CdS nanowires.

To evaluate the stability of the CdS/g-$C_3N_4$ core/shell nanowires, recycling rest was performed on the hydrogen-production activity of the sample CN2. Figure 6 displays the

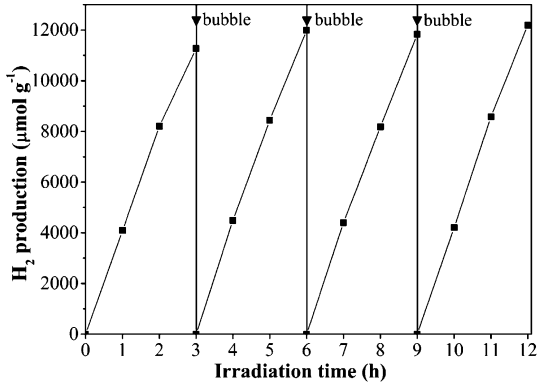


**Figure 6.** Time course of photocatalytic $H_2$ production for sample CN2. The reaction system was bubbled with $N_2$ for 30 min every 3 h to remove the $H_2$ inside.

$H_2$-production performance in a cycling photocatalytic run. After four recycles, there is no decrease observed in the $H_2$-production rate, indicating the good stability of the catalyst during the photocatalytic reaction. In addition, it can be found that after the first cycle, the average $H_2$-production rate is slightly inceased because the hydrogen-production reaction is an activated process, and the photons absorbed on the surface of the photocatalyst increase with increasing irradiation time.[53] However, for future practical applications, the photostability of the g-$C_3N_4$-coated nanowires in a nonsacrificial system should be more important. Therefore, we compared the photocorrosion behaviors of the pristine (CN0) and 2 wt % g-$C_3N_4$-coated (CN2) CdS nanowires in anaerobic distilled water under the irradiation of a 350 W xenon arc lamp. It is reported that the photocorrosion reaction of CdS in an anaerobic aqueous system can be presented as follows:[21]

$$CdS + 2h^+ \rightarrow Cd^{2+} + S \quad (2)$$

Thus, photogenerated holes destroy the crystal structure of CdS, and $Cd^{2+}$ ions were released in water. The concentrations of $Cd^{2+}$ in the solution of the pristine (CN0) and 2 wt % g-$C_3N_4$-coated (CN2) CdS nanowires after irradiation for different time intervals are listed in Table 2. As shown in

**Table 2. Concentrations of $Cd^{2+}$ ($mg\ L^{-1}$) in the Solutions of Pristine (CN0) and 2 wt % g-$C_3N_4$-Coated (CN2) CdS Nanowires in Anaerobic Water Before (0 h) and after Irradiation**

| | irradiation time (h) | | | |
|---|---|---|---|---|
| sample | 0 | 1 | 4 | 8 |
| CN0 | 0.40 | 18.16 | 232.76 | 329.23 |
| CN2 | 0.88 | 2.26 | 7.33 | 29.04 |

Table 2, the pristine CdS exhibits a greater dissolution rate under light irradiation. After 8 h of irradiation, most of the CdS was decomposited, and the concentration of released $Cd^{2+}$ in solution reached 329.23 mg $L^{-1}$. The residual solids in the reacted solution were collected and characterized by TEM imaging. As displayed in Figure 7a, the morphology and crystal structure of the nanowires are obviously destroyed, leaving a


dx.doi.org/10.1021/am403327g | ACS Appl. Mater. Interfaces 2013, 5, 10317−10324

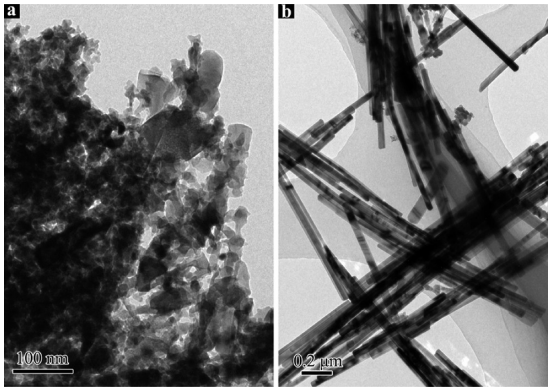


**Figure 7.** Comparison of the TEM images for (a) pristine CdS nanowires and (b) 2 wt % g-$C_3N_4$-coated CdS nanowires after 8 h of light irradiation in anaerobic distilled water.

porous aggregation. In contrast, for g-$C_3N_4$-coated CdS nanowires (CN2), the dissolution trend is significantly retarded. The concentration of released $Cd^{2+}$ in the reaction solution is only about 29.04 mg $L^{-1}$ after 8 h of light irradiation. TEM observation (Figure 7b) further indicates that the morphology and crystal structure of the g-$C_3N_4$-hybridized nanowires were essentially unchanged during the photocorrosion test. Evidently, coating g-$C_3N_4$ on the surface of CdS could greatly inhibit the damage of photocorrosion and enhance the stability of the CdS photocatalyst.

**Mechanism of Enhancement of Photocatalytic Activity and Suppression of Photocorrosion.** It is generally accepted that photocatalytic activity is mainly governed by light-absorption ability, surface properties (including adsorption property, specific surface area, etc.), and photogenerated charge-separation efficiency.[1] For CdS nanowires, the photocatalytic hydrogen-production rate can be improved by over 2-fold via 2 wt % g-$C_3N_4$ coating. However, as discussed above, the g-$C_3N_4$ coating did not substantially influence the light-absorption property and specific surface area (20.5 $m^2$ $g^{-1}$ for CN0 and 22.9 $m^2$ $g^{-1}$ for CN2) of the nanowires, indicating that these two factors are not crucial to the photocatalytic activity for CdS/g-$C_3N_4$ core/shell nanowires. Therefore, the enhanced photocatalytic activities of g-$C_3N_4$-coated CdS nanowires may be mainly attributed to the synergic effect between g-$C_3N_4$ and CdS, which can greatly accelerate the separation of photogenerated carriers. The schematic representation of the energy-level configuration and the photogenerated charge-transfer process in g-$C_3N_4$/CdS composites is illustrated in Figure 8a. It is reported that the lowest unoccupied molecular orbital (LUMO) and highest occupied molecular orbital (HOMO) levels of g-$C_3N_4$ are higher than the corresponding conduction band minimun (CBM) and valence band maximum (VBM) of CdS, respectively.[45] Under the excitation of visible light, the photogenerated electrons on the LUMO level of g-$C_3N_4$ can be readily injected in the conduction band of CdS, whereas the photogenerated holes on VBM of CdS can directly transfer to the HOMO of g-$C_3N_4$. Therefore, when a small amount ($R_{CN}$ < 2 wt %) of g-$C_3N_4$ is coated on the CdS nanowires, the excited energetic electrons on g-$C_3N_4$ can be injected to CdS and then participate in the photocatalytic hydrogen-evolution reaction on the uncovered tips and areas of CdS together with the photogenerated electrons on CdS (Figure 8b). Meanwhile, the photogenerated holes on CdS can rapidly migrate to the coated g-$C_3N_4$ and

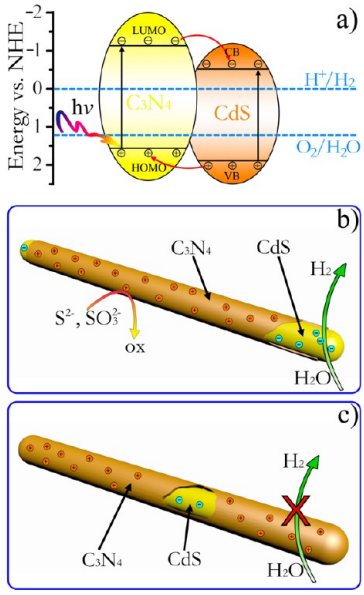


**Figure 8.** Schematic illustration of (a) the energy-level configuration and the photogenerated charge-transfer process between g-$C_3N_4$ and CdS, (b) the photocatalytic process on a CdS nanowire with a thin and unclosed g-$C_3N_4$ shell, and (c) a CdS nanowire with a dense and closed g-$C_3N_4$ shell.

thus substantially alleviate the photocorrosion of CdS. In this case, an effective charge separation can be achieved, resulting in enhancement of photocatalytic activity and inhibition of photocorrosion. However, as the content of g-$C_3N_4$ increases, a dense and closed shell around the CdS nanowire is gradually formed (Figure 8c). In such a situation, the closed shell prevents CdS from contacting the reaction solution. Thus, electrons in CdS cannot participate in the hydrogen-evolution reaction and will accumulate on the interface of g-$C_3N_4$ and CdS, which may lead to a serious recombination of photogenerated electron-hole pairs. Consequently, the synergic effect between g-$C_3N_4$ and CdS diminishes drastically and the photocatalytic activity will decrease rapidly with further increasing of the g-$C_3N_4$ content.

Photoelectrochemical measurements are often used to qualitatively study the excitation and transfer of photogenerated charge carriers in photocatalysts. The transient photocurrent responses of the pristine, 2 wt % g-$C_3N_4$-coated, and 4 wt % g-$C_3N_4$-coated CdS nanowires were recorded for several on−off cycles under visible-light irradiation and are plotted in Figure 9. As expected, 2 wt % g-$C_3N_4$-coated CdS nanowires show the highest photocurrent intensity of the three samples, whereas pristine CdS and 4 wt % g-$C_3N_4$-coated CdS have the middle and lowest values, respectively. Thus, the sample with 2 wt % g-$C_3N_4$ may achieve the most effective charge separation, which is consistent with the photocatalytic-activity measurements and our above discussions.

## CONCLUSIONS

We have successfully synthesized CdS/g-$C_3N_4$ core/shell nanowires by a combined solvothermal and chemisorption method. The photocatalytic hydrogen-production rates of the CdS nanowires are significantly enhanced in the presence of the g-$C_3N_4$ shell and reach the maximum value at $R_{CN}$ = 2 wt %. At the optimal loading content (2 wt %), g-$C_3N_4$ formed thin and unclosed shells on CdS nanowires, and the hydrogen-

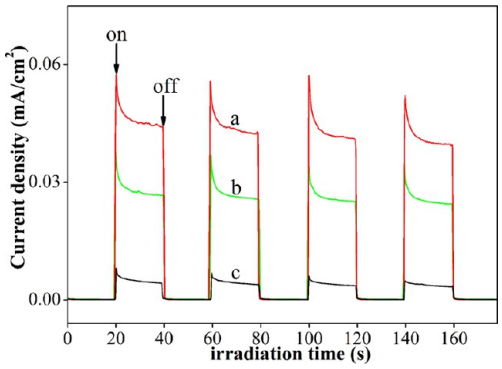


**Figure 9.** Transient photocurrent responses of CN2 (a), CN0 (b), and CN4 (c) in a 0.5 M $Na_2SO_4$ aqueous solution under visible-light irradiation at 0.0 V using Ag/AgCl as a reference electrode.

production rate is up to 4152 $\mu$mol $h^{-1}g^{-1}$ with an apparent quantum efficiency (QE) up to 4.3% at 420 nm. More importantly, the CdS/g-$C_3N_4$ core/shell nanowires exhibit excellent photostability even though they were irradiated in a nonsacrifical system. According to our discussion, the enhanced photocatalytic activity and intensified photostability may be ascribed to the synergic effect between g-$C_3N_4$ and CdS originating from their well-matched overlapping band structures, which can effectively accelerate the charge separation and transfer corrosive holes from CdS to robust $C_3N_4$. It should be noted that in such a CdS/g-$C_3N_4$ core/shell configuration the exposure of CdS to the reaction solution is a necessary condition for the synergic effect to be effective. For CdS nanowires with dense and closed $C_3N_4$ shells, the photocatalytic activity is seriously depressed. The CdS/g-$C_3N_4$ core/shell nanowires introduced in this work, with high photocatalytic activity and excellent photostability, are a very promising candidate for possible practical application in high-performance $H_2$ production. Furthermore, the proposed mechanisms for the photocatalytic hydrogen-evolution process may also provide some ideas for the future design of new photocatalysts with similar core/shell structures.

## ■ ASSOCIATED CONTENT

### Supporting Information

TEM images for g-$C_3N_4$ sheets after ultrasonic treatment, EDS and XPS spectra for the g-$C_3N_4$ coated CdS nanorods, and schematic illustration of the formation process of CdS/g-$C_3N_4$ core/shell structures. This material is available free of charge via the Internet at http://pubs.acs.org.

## ■ AUTHOR INFORMATION

### Corresponding Authors

*E-mail: fhuang@fjirsm.ac.cn (F.H.).
*E-mail: jiaguoyu@yahoo.com (J.Y.).

### Author Contributions

The manuscript was written through contributions of all authors. All authors have given approval to the final version of the manuscript.

### Notes

The authors declare no competing financial interest.

## ■ ACKNOWLEDGMENTS

This work was supported by the National Basic Research Program of China (973 Program, nos. 2010CB933501 and 2013CB934302), the National Natural Science Foundation of China (nos. 51102232, 20971123, and 21007070), the Fujian National Natural Science Foundation of China (nos. 2010J01054 and 2010J06006), the NNSF Outstanding Youth Fund (nos. 21125730 and 50625205), and the Knowledge Innovation Program of the Chinese Academy of Sciences (nos. KJCX2-YW-N50 and KJCX2-EW-J02).

## ■ REFERENCES

(1) Kudo, A.; Miseki, Y. *Chem. Soc. Rev.* **2009**, *38*, 253−278.
(2) Listorti, A.; Durrant, J.; Barber, J. *Nat. Mater.* **2009**, *8*, 929−930.
(3) Gray, H. B. *Nat. Chem.* **2009**, *1*, 7−7.
(4) Tollefson, J. *Nature* **2010**, *464*, 1262−1264.
(5) Gamelin, D. R. *Nat. Chem.* **2012**, *4*, 965−967.
(6) Sanderson, K. *Nature* **2008**, *452*, 400−402.
(7) Zhou, H.; Guo, J. J.; Li, P.; Fan, T. X.; Zhang, D.; Ye, J. H. *Sci. Rep.* **2013**, *3*, 1667-1−1667-9.
(8) Prieto, G.; Zecevic, J.; Friedrich, H.; de Jong, K. P.; de Jongh, P. E. *Nat. Mater.* **2013**, *12*, 34−39.
(9) In, S. I.; Vaughn, D. D.; Schaak, R. E. *Angew. Chem., Int. Ed.* **2012**, *51*, 3915−3918.
(10) Cheng, H. F.; Huang, B. B.; Liu, Y. Y.; Wang, Z. Y.; Qin, X. Y.; Zhang, X. Y.; Dai, Y. *Chem. Commun.* **2012**, *48*, 9729−9731.
(11) Dahl, S.; Chorkendorff, I. *Nat. Mater.* **2012**, *11*, 100−101.
(12) Kandiel, T. A.; Ismail, A. A.; Bahnemann, D. W. *Phys. Chem. Chem. Phys.* **2011**, *13*, 20155−20161.
(13) Wen, C. Z.; Hu, Q. H.; Guo, Y. N.; Gong, X. Q.; Qiao, S. Z.; Yang, H. G. *Chem. Commun.* **2011**, *47*, 6138−6140.
(14) Yu, J. G.; Qi, L. F.; Jaroniec, M. *J. Phys. Chem. C* **2010**, *114*, 13118−13125.
(15) Tu, W. G.; Zhou, Y.; Liu, Q.; Tian, Z. P.; Gao, J.; Chen, X. Y.; Zhang, H. T.; Liu, J. G.; Zou, Z. G. *Adv. Funct. Mater.* **2012**, *22*, 1215−1221.
(16) Liu, L. J.; Zhao, H. L.; Andino, J. M.; Li, Y. *ACS Catal.* **2012**, *2*, 1817−1828.
(17) Zhang, J. Y.; Wang, Y. H.; Zhang, J.; Lin, Z.; Huang, F.; Yu, J. G. *ACS Appl. Mater. Interfaces* **2013**, *5*, 1031−1037.
(18) Zhang, J.; Yu, J. G.; Zhang, Y. M.; Li, Q.; Gong, J. R. *Nano Lett.* **2011**, *11*, 4774−4779.
(19) Hong, Y. P.; Zhang, J.; Wang, X.; Wang, Y. J.; Lin, Z.; Yu, J. G.; Huang, F. *Nanoscale* **2012**, *4*, 2859−2862.
(20) Fujiwara, H.; Hosokawa, H.; Murakoshi, K.; Wada, Y.; Yanagida, S. *Langmuir* **1998**, *14*, 5154−5159.
(21) Chen, X. B.; Shen, S. H.; Guo, L. J.; Mao, S. S. *Chem. Rev.* **2010**, *110*, 6503−6570.
(22) Ran, J. R.; Yu, J. G.; Jaroniec, M. *Green Chem.* **2011**, *13*, 2708−2713.
(23) Li, Q.; Guo, B. D.; Yu, J. G.; Ran, J. R.; Zhang, B. H.; Yan, H. J.; Gong, J. R. *J. Am. Chem. Soc.* **2011**, *133*, 10878−10884.
(24) Yan, X. X.; Liu, G.; Wang, L. Z.; Wang, Y.; Zhu, X. F.; Zou, J.; Lu, G. Q. *J. Mater. Res.* **2010**, *25*, 182−188.
(25) Qi, L. F.; Yu, J. G.; Jaroniec, M. *Phys. Chem. Chem. Phys.* **2011**, *13*, 8915−8923.
(26) Li, B. X.; Wang, Y. F. *J. Phys. Chem. Solids* **2011**, *72*, 1165−1169.
(27) Xu, L. L.; Shi, W. D.; Guan, J. G. *Catal. Commun.* **2012**, *25*, 54−58.
(28) Wang, Y. B.; Wang, Y. S.; Xu, R. *J. Phys. Chem. C* **2013**, *117*, 783−790.
(29) Wu, K. F.; Zhu, H. M.; Liu, Z.; Rodriguez-Cordoba, W.; Lian, T. Q. *J. Am. Chem. Soc.* **2012**, *134*, 10337−10340.
(30) Hu, Y.; Gao, X.; Yu, L.; Wang, Y.; Ning, J.; Xu, S.; Lou, X. W. *Angew. Chem., Int. Ed.* **2013**, 5636−5639.
(31) Zhang, H.; Zhu, Y. F. *J. Phys. Chem. C* **2010**, *114*, 5822−5826.
(32) Pan, B.; Xie, Y.; Zhang, S.; Lv, L.; Zhang, W. *ACS Appl. Mater. Interfaces* **2012**, *4*, 3938−3943.
(33) Kalyanasundaram, K.; Borgarello, E.; Duonghong, D.; Gratzel, M. *Angew. Chem., Int. Ed. Engl.* **1981**, *20*, 987−988.

(34) Zheng, Y.; Liu, J.; Liang, J.; Jaroniec, M.; Qiao, S. Z. *Energy Environ. Sci.* **2012**, *5*, 6717−6731.
(35) Wang, Y.; Wang, X. C.; Antonietti, M. *Angew. Chem., Int. Ed.* **2012**, *51*, 68−89.
(36) Zhang, J. S.; Chen, X. F.; Takanabe, K.; Maeda, K.; Domen, K.; Epping, J. D.; Fu, X. Z.; Antonietti, M.; Wang, X. C. *Angew. Chem., Int. Ed.* **2010**, *49*, 441−444.
(37) Zhang, Y. J.; Antonietti, M. *Chem.−Asian J.* **2010**, *5*, 1307−1311.
(38) Tian, J. Q.; Liu, Q.; Asiri, A. M.; Al-Youbi, A. O.; Sun, X. P. *Anal. Chem.* **2013**, *85*, 5595−5599.
(39) Cheng, N. Y.; Tian, J. Q.; Liu, Q.; Ge, C. J.; Qusti, A. H.; Asiri, A. M.; Al-Youbi, A. O.; Sun, X. P. *ACS Appl. Mater. Interfaces* **2013**, *5*, 6815−6819.
(40) Tian, J. Q.; Liu, Q.; Ge, C. J.; Xing, Z. C.; Asiri, A. M.; Al-Youbi, A. O.; Sun, X. P. *Nanoscale* **2013**, *5*, 8921−8924.
(41) Zhang, Y. J.; Mori, T.; Niu, L.; Ye, J. H. *Energy Environ. Sci.* **2011**, *4*, 4517−4521.
(42) Pan, C. S.; Xu, J.; Wang, Y. J.; Li, D.; Zhu, Y. F. *Adv. Funct. Mater.* **2012**, *22*, 1518−1524.
(43) Wang, Y. J.; Shi, R.; Lin, J.; Zhu, Y. F. *Energy Environ. Sci.* **2011**, *4*, 2922−2929.
(44) Fu, J.; Chang, B. B.; Tian, Y. L.; Xi, F. N.; Dong, X. P. *J. Mater. Chem. A* **2013**, *1*, 3083−3090.
(45) Cao, S. W.; Yuan, Y. P.; Fang, J.; Shahjamali, M. M.; Boey, F. Y. C.; Barber, J.; Loo, S. C. J.; Xue, C. *Int. J. Hydrogen Energy* **2013**, *38*, 1258−1266.
(46) Ge, L.; Zuo, F.; Liu, J. K.; Ma, Q.; Wang, C.; Sun, D. Z.; Bartels, L.; Feng, P. Y. *J. Phys. Chem. C* **2012**, *116*, 13708−13714.
(47) Hwang, S. H.; Kim, C.; Song, H.; Son, S.; Jang, J. *ACS Appl. Mater. Interfaces* **2012**, *4*, 5287−5292.
(48) Jang, J. S.; Joshi, U. A.; Lee, J. S. *J. Phys. Chem. C* **2007**, *111*, 13280−13287.
(49) Dong, G. H.; Zhang, L. Z. *J. Mater. Chem.* **2012**, *22*, 1160−1166.
(50) Bai, X. J.; Wang, L.; Zong, R. L.; Zhu, Y. F. *J. Phys. Chem. C* **2013**, *117*, 9952−9961.
(51) Li, X. M.; Zhu, H. W.; Wei, J. Q.; Wang, K. L.; Xu, E. Y.; Li, Z.; Wu, D. H. *Appl. Phys. A: Mater. Sci. Process.* **2009**, *97*, 341−344.
(52) Sing, K. S. W.; Everett, D. H.; Haul, R. A. W.; Moscou, L.; Pierotti, R. A.; Rouquerol, J.; Siemieniewska, T. *Pure Appl. Chem.* **1985**, *57*, 603−619.
(53) Zhang, J.; Liu, S. W.; Yu, J. G.; Jaroniec, M. *J. Mater. Chem.* **2011**, *21*, 14655−14662.